
Unsupervised Learning on Neural Network Outputs

Yao Lu

Department of Computer Science, University of Helsinki
 Department of Mathematics and Statistics, University of Helsinki
 Helsinki Institute for Information Technology HIIT, Finland
 yaolubrain@gmail.com

Abstract

The outputs of a trained neural network contain much richer information than just an one-hot classifier. For example, a neural network may give an image of a dog the probability of one in a million of being a cat but it is still much larger than the probability of being a car. To reveal the hidden structure in them, we apply two unsupervised learning algorithms, PCA and ICA, to the outputs of a deep convolutional neural network trained on the ImageNet of 1000 classes. The PCA/ICA embedding of the object classes reveals their visual similarity and the PCA/ICA components can be interpreted as common features shared by visually similar object classes. For an application, we show that the learned PCA/ICA can be useful for zero-shot learning. Our new zero-shot learning method outperforms previous state-of-the-art methods on the ImageNet of over 20000 classes.

1 Introduction

Recently, Deep Convolutional Neural Network (DCNN) [1] has made significant advances in computer vision [2, 3]. Moreover, DCNN also sheds lights on neural coding in visual cortex. In [4], it has been shown that a trained DCNN rivals the representational performance of inferior temporal cortex on a visual object recognition task. Therefore, investigating the properties of a trained DCNN is important for both computer vision applications and discovering the principles of neural coding in the brain.

In [5], Hinton et al. showed that the softmax outputs of a trained neural network contain much richer information than just a one-hot classifier. For input vector $\mathbf{y} = (y_1, \dots, y_n)$, which is called logits in [5], the softmax function produces output vector $\mathbf{x} = (x_1, \dots, x_n)$ such that

$$x_i = \frac{\exp(y_i/T)}{\sum_j \exp(y_j/T)} \quad (1)$$

where T is the temperature parameter. The softmax function assigns positive probabilities to all classes since $x_i > 0$ for all i . Given a data point of a certain class as input, even when the probabilities of the incorrect classes are small, some of them are much larger than the others. For example, in a 4-class classification task (cow, dog, cat, car), given an image of a dog, while a hard target (class label) is $(0, 1, 0, 0)$, a trained neural network might output a soft target $(10^{-6}, 0.9, 0.1, 10^{-9})$. An image of a dog might have small chance to be misclassified as cat but it is much less likely to be misclassified as car. In [5], a technique called knowledge distillation was introduced to further reveal the information in the softmax outputs. Knowledge distillation raises the temperature T in the softmax function to soften the outputs. For example, it transforms $(10^{-6}, 0.9, 0.1, 10^{-9})$ to $(0.015, 0.664, 0.319, 0.001)$ by raising temperature T from 1 to 3. It has been shown that adding the distilled soft targets in the objective function helps in reducing generalization error when training a smaller model of an ensemble of models [5]. Therefore, the outputs of a trained neural network are far from one-hot hard targets or random noise and they might contain rich statistical structures.

In this paper, to explore the information hidden in the outputs, we apply two unsupervised learning algorithms, Principle Component Analysis (PCA) and Independent Component Analysis (ICA) [6] to the outputs of a DCNN trained on the ImageNet dataset [7]. Both PCA and ICA are special cases of Factor Analysis, with different assumptions on the latent variables. Factor Analysis is a statistical model which can be used for revealing hidden factors that underlie a vector of random variables. In the case of DCNN for object recognition, the neurons in the output layer of a DCNN, as random variables, stand for object classes. A latent factor might represent a common visual attribute shared by several object classes. It is therefore desirable to visualize and interpret the Factor Analysis model learned on the outputs of a trained DCNN.

2 Softmax

Because a DCNN was trained with one-hot hard targets (class labels), given a training image as input, the softmax function suppresses the outputs of most neurons in the output layer and leaves one or a few peak values. For example, in Figure 1 (a), we show the softmax ($T = 1$) outputs for a training image. To magnify the tiny values in the softmax outputs, after a DCNN was trained with softmax function ($T = 1$), we take the logits y in e.q. (1) and apply the following normalization function

$$x_i = \frac{(y_i - \min_k y_k)}{\sum_j (y_j - \min_k y_k)} \quad (2)$$

for all i , as the outputs of the DCNN, with all the parameters in the DCNN unchanged. This function normalizes y so that x in eq. (2) is still a probability distribution over classes. We call the x in eq. (2) normalized logits. In Figure 1 (b), we show the outputs of this function given the same input image as Figure 1 (a).

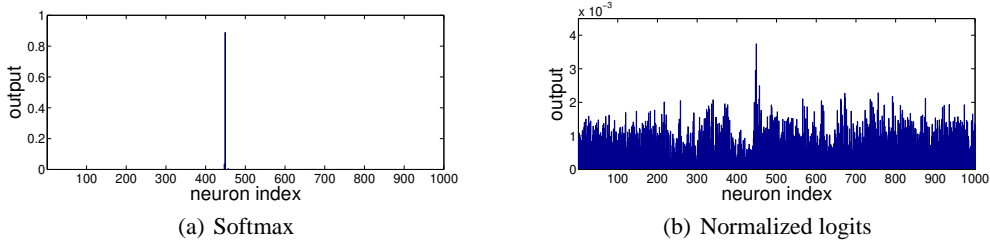


Figure 1: Outputs

In order to apply ICA, the variables must not all be Gaussian. The non-gaussianity of a random variable x of zero mean can be measured by kurtosis $E(x^4)/E(x^2)^2 - 3$, which is zero if x is Gaussian. We computed the kurtosis of the outputs (mean removed) of a DCNN with softmax and normalized logits using all the ImageNet ILSVRC2012 training data. The DCNN model and experimental settings are described in Section 4. The result is, all neurons in the output layer have positive kurtosis, as shown in Figure 2. Therefore the neurons as random variables are highly non-gaussian and it is sensible to apply ICA, which is introduced in the next section.

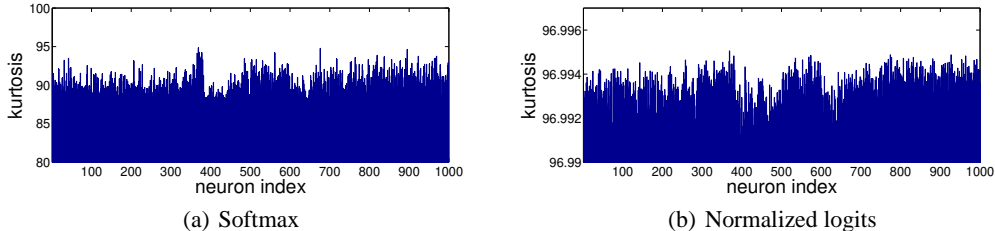


Figure 2: Kurtosis

3 Factor Analysis

In Factor Analysis, we assume the observed variables $\mathbf{x} = (x_1, \dots, x_n)$ are generated by the following model

$$\mathbf{x} = \mathbf{A}\mathbf{s} + \mathbf{n} \quad (3)$$

where $\mathbf{s} = (s_1, \dots, s_n)$ are the latent variables, \mathbf{A} is the model parameter matrix and \mathbf{n} are the noise variables. Here, \mathbf{x} and \mathbf{s} are assumed to have zero-mean. \mathbf{s} are also assumed to be uncorrelated and have unity variance, in other words, white.

3.1 Principle Component Analysis

Principle Component Analysis (PCA) is a special case of Factor Analysis. In PCA, \mathbf{s} are assumed to be Gaussian and \mathbf{n} are assumed to be zero (noise-free). Let \mathbf{C} denote the covariance matrix of \mathbf{x} , $\mathbf{E} = (\mathbf{e}_1, \dots, \mathbf{e}_n)$ denotes the matrix of eigenvectors of \mathbf{C} and $\mathbf{D} = \text{diag}(\lambda_1, \dots, \lambda_n)$ denotes the diagonal matrix of eigenvalues of \mathbf{C} . The PCA matrix is \mathbf{E}^T , the whitening matrix is $\mathbf{U} = \mathbf{D}^{-1/2}\mathbf{E}^T$ and the whitened variables are $\mathbf{z} = \mathbf{U}\mathbf{x}$.

3.2 Independent Component Analysis

Independent Component Analysis (ICA) [6] is another special case of Factor Analysis. In ICA, \mathbf{s} are assumed to be non-gaussian and independent and \mathbf{n} are assumed to be zero. ICA seeks a demixing matrix \mathbf{W} such that $\mathbf{W}\mathbf{x}$ can be as independent as possible. To obtain \mathbf{W} , we can first decompose it as $\mathbf{W} = \mathbf{V}\mathbf{U}$, where \mathbf{U} is the whitening matrix and \mathbf{V} is an orthogonal matrix, which can be learned by maximizing the non-gaussianity or the likelihood function of $\mathbf{V}\mathbf{U}\mathbf{x}$. The non-gaussianity can be measured by kurtosis or negentropy. If dimensionality reduction is required, we can take the d largest eigenvalues and the corresponding eigenvectors for the whitening matrix \mathbf{U} . As a result, the size of \mathbf{U} is $d \times n$ and the size of \mathbf{V} is $d \times d$. ICA is ambiguous of scaling each component. If \mathbf{W} is an ICA demixing matrix, then $\text{diag}(\alpha_1, \dots, \alpha_d)\mathbf{W}$ is also an ICA demixing matrix, where $\{\alpha_1, \dots, \alpha_d\}$ are non-zero scaling constants of the components.

A classic ICA algorithm is FastICA [8]. Despite its fast convergence, FastICA is a batch algorithm which requires all the data to be loaded for computation in each iteration. Thus, it is unsuitable for large scale applications. To handle large scale datasets, we use a stochastic gradient descent (SGD) based ICA algorithm (described in the Appendix of [8] and Section 3.4 of [9]). For samples $\{\mathbf{z}(1), \mathbf{z}(2), \dots\}$, one updating step of the SGD-based algorithm of a given sample $\mathbf{z}(t)$ is:

$$\mathbf{V} \leftarrow \mathbf{V} + \mu g(\mathbf{V}\mathbf{z}(t))\mathbf{z}(t)^T + \frac{1}{2}(\mathbf{I} - \mathbf{V}\mathbf{V}^T)\mathbf{V}^T \quad (4)$$

where μ is the learning rate, $g(\cdot) = -\tanh(\cdot)$ and \mathbf{I} is an identity matrix. In our experiments, \mathbf{V} was initialized as a random orthogonal matrix.

Like FastICA, this SGD-based algorithm requires going through all data once to compute the whitening matrix \mathbf{U} . But unlike FastICA, this SGD-based algorithm does not require projection or orthogonalization in each step.

In this algorithm, the assumption on the probability distribution of each s_i is a super-gaussian distribution

$$\log p(s_i) = -\log \cosh(s_i) + \text{constant} \quad (5)$$

and therefore

$$g(s_i) = \frac{\partial}{\partial s_i} \log p(s_i) = -\tanh(s_i). \quad (6)$$

Since the variables obtained by linear transformations of Gaussian variables are also Gaussian, from Section 2, we can infer at least some of the latent variables of the neurons in the output layer are non-gaussian, under the noise-free Factor Analysis assumption. However, there are an infinite number of non-gaussian probability distributions. As an initial attempt, we choose a particular one here. Explorations of different non-gaussian distributions and therefore different nonlinearities $g(\cdot)$ are left for future research.

4 Results

4.1 Experimental Settings

The trained DCNN model used in the experiments consists of 5 convolution layers, 2 fully connected layer and 1 softmax output layer, as described in ¹. The model was trained on the ImageNet ILSVRC2012 training set of 1.28 million images and 1000 classes. It achieves 37.3% top-1 error rate and 15.5% top-5 error rate in ImageNet ILSVRC2012 validation set, which outperforms any single model in [3, 10]. The outputs of the DCNN were computed with Toronto Deep Learning ² toolkit. We used all the images in the ImageNet ILSVRC2012 training set to compute the ICA matrix using our SGD-based algorithm with mini-batch size 500. The learning rate was set to 0.005 and was halved every 10 epochs. The ICA algorithm was ran with Theano [11].

4.2 Visualization of PCA/ICA components

To understand what is learned with PCA and ICA, we visualize the PCA and the ICA matrix. In the PCA matrix \mathbf{E}^T or ICA matrix \mathbf{W} , each row corresponds to a PCA/ICA component and each column corresponds to an object class. The number of rows depends on the dimensionality reduction. The number of columns of \mathbf{E}^T or \mathbf{W} is 1000, corresponding to 1000 classes. After the ICA matrix was learned, each ICA component (a row of \mathbf{W}) was scaled to have unity l_2 norm. The scaling of each ICA component does not affect the ICA solution, as discussed in Section 3.2.

In Figure 3, we show the embedding of class labels by PCA and ICA. The horizontal and the vertical axes are two distinct rows of \mathbf{E}^T or \mathbf{W} . Each point in the plot corresponds to an object class. And there are 1000 points in each plot. Dimensionality is reduced from 1000 to 200 in ICA. In Figure 3 (a) and (b), we plot two pairs of the ICA/PCA components, learned with softmax outputs. In the PCA embedding, visually similar class labels are along some lines, but not the axes, while in the ICA embedding, they are along the axes. However, most points are clustered in the origin. In Figure 3 (c) and (d), we plot two pairs of the ICA/PCA components, learned with normalized logits outputs. We can see the class labels are more scattered in the plots.

In Table 1, we show the top-5 object classes according to the value of PCA and ICA components. For the ease of comparison, we selected each PCA or ICA component which has the largest value for class *mosque*, *killer whale*, *Model T* or *zebra* among all components. We can see that the class labels ranked by ICA components are more visually similar than the ones by PCA components.

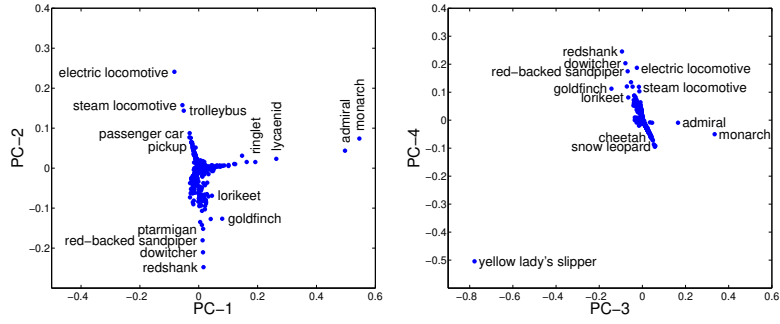
The PCA/ICA components can be interpreted as common features shared by visually similar object classes. From Figure 3 and Table 1, we can see the label embeddings of object classes by PCA/ICA components are meaningful since visually similar classes are close in the embeddings. Unlike [12], these label embeddings can be unsupervisedly learned with a DCNN trained with only one-hot class labels and without any hand annotated attribute label of the object classes, such as *has tail* or *lives in the sea*.

Table 1: Object classes ranked by single components of PCA/ICA

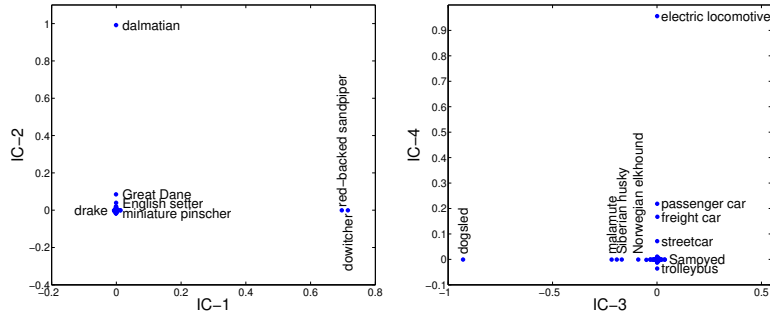
	1	2	3	4
PCA	mosque airship volcano dome golfcart	killer whale pomegranate tarantula shark grey whale green snake	Model T radio telescope trilobite basketball lifeboat	zebra giant panda hartebeest impala manhole cover
ICA	mosque castle planetarium dome church	killer whale grey whale speed boat sea lion submarine	Model T golfcart tractor motor scooter thresher	zebra park bench hyena warthog gazelle

¹https://github.com/TorontoDeepLearning/convnet/blob/master/examples/imagenet/CLS_net_201408

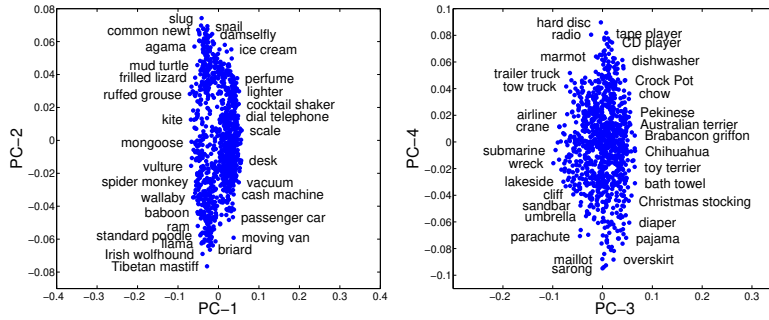
²<https://github.com/TorontoDeepLearning/convnet>



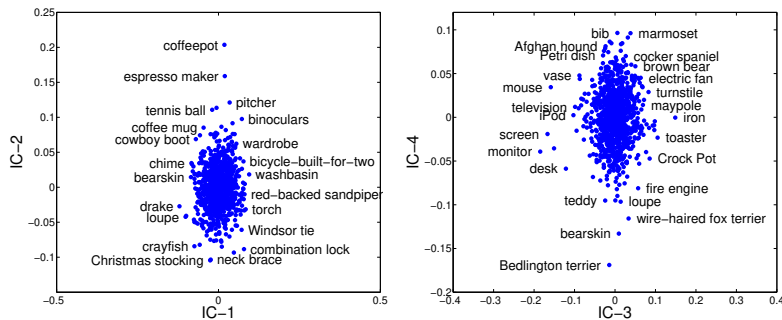
(a) PCA, softmax.



(b) ICA, softmax.



(c) PCA, normalized logits.



(d) ICA, normalized logits.

Figure 3: Label embedding of object class by PCA/ICA components. In each plot, each point is an object class and each axis is a PCA/ICA component (PC/IC). For visual clarity, only selected points are annotated with object class labels.

4.3 Visual vs. Semantic Similarity

The visual-semantic similarity relationship was previously explored in [13], which shows some consistency between two similarities. Here we further explore it from another perspective. We define the visual and the semantic similarity in the following way. The visual similarity between two object classes is defined as cosine similarity of their PCA or ICA components (200-dim and learned with softmax), both of which give the same results. The semantic similarity is defined based on the shortest path length³ between two classes on the WordNet graph [14]. In Table 2, we compare five closest classes of *Egyptian cat*, *soccer ball*, *mushroom* and *red wine* in terms of visual and semantic similarity. For *Egyptian cat*, both visual and semantic similarities give similar results. For *soccer ball*, the visual similarity gives *football helmet* which is quite distant in terms of semantic similarities. For *mushroom* and *red wine*, two similarities give very different closest object classes. The gap between two similarities is intriguing and therefore worth further exploration. In neuroscience literature, it is claimed that visual cortex representation favors visual rather than semantic similarity [15].

Table 2: Closest object classes in terms of visual and semantic similarity

	Egyptian cat	soccer ball	mushroom	red wine
Visual	tabby cat	rugby ball	agaric	wine bottle
	tiger cat	football helmet	bolete	goblet
	tiger	croquet ball	hen-of-the-woods	beaker
	lynx	racket	earthstar	beer glass
	Persian cat	tennis ball	slug	measuring cup
Semantic	Persian cat	croquet ball	cucumber	eggnog
	tiger cat	golf ball	artichoke	cup
	Siamese cat	baseball	cardoon	espresso
	tabby cat	ping-pong ball	broccoli	menu
	cougar	punching bag	cauliflower	meat loaf

5 Application: Zero-shot Learning

The zero-shot learning [16, 17, 18] task is to classify images whose class labels are not in the training set (unseen). It uses semantic knowledge of classes, such as attributes, to extrapolate the unseen classes. Previous state-of-the-art large scale zero-shot learning methods, which use the ImageNet of 1000 classes for training and the ImageNet of over 20000 classes for testing, are DeViSE [19] and conSE [20]. Both methods use a supervised DCNN for image representation and unsupervised learning (word2vec [21]) to learn a semantic representation of object classes from text corpus (Wikipedia). Our method differs from them by using unsupervised learning algorithms to learn: (1) a visual representation of classes. (2) a semantic representation of classes from the WordNet graph. (3) a bridge between the visual and semantic representations.

Our method works as follows. First, assume we have obtained the visual feature vectors $\mathbf{W}^{(1)} = (\mathbf{w}_1^{(1)}, \dots, \mathbf{w}_n^{(1)})$ of n seen classes. Let $\mathbf{M} = (\mathbf{m}_1, \dots, \mathbf{m}_n)$ denotes the matrix of the mean outputs of a DCNN of the seen classes. And $\mathbf{F} = f(\mathbf{W}^{(1)}\mathbf{M}) = (\mathbf{f}_1, \dots, \mathbf{f}_n)$ are the transformed mean outputs of the seen classes, where $f(\cdot)$ is a nonlinear function. Next, assume we have obtained the semantic feature vectors $\mathbf{W}^{(2)} = (\mathbf{w}_1^{(2)}, \dots, \mathbf{w}_n^{(2)})$ of n seen classes and $\mathbf{W}^{(3)} = (\mathbf{w}_1^{(3)}, \dots, \mathbf{w}_m^{(3)})$ of m unseen classes. Due to the visual-semantic similarity gap shown in Section 4.3, we learn a bridge between the visual and the semantic representations of object classes via Canonical Correlation Analysis (CCA) [22]. which seeks two projection matrices $\mathbf{P}^{(1)}$ and $\mathbf{P}^{(2)}$ such that

$$\min_{\mathbf{P}^{(1)}, \mathbf{P}^{(2)}} \|\mathbf{P}^{(1)T}\mathbf{F} - \mathbf{P}^{(2)T}\mathbf{W}^{(2)}\|_F \quad (7)$$

$$\text{s.t. } \mathbf{P}^{(k)T}\mathbf{C}_{kk}\mathbf{P}^{(k)} = \mathbf{I}, \quad \mathbf{p}_i^{(k)T}\mathbf{C}_{kl}\mathbf{p}_j^{(l)} = 0, \quad (8)$$

$$k, l = 1, 2, \quad k \neq l, \quad i, j = 1, \dots, d, \quad (9)$$

³computed with the path_similarity() function in the NLTK tool <http://www.nltk.org/howto/wordnet.html>

where $\mathbf{p}_i^{(k)}$ is the i -th column of $\mathbf{P}^{(k)}$ and \mathbf{C}_{kl} is a covariance or cross-covariance matrix of $\{\mathbf{f}_1, \dots, \mathbf{f}_n\}$ and/or $\{\mathbf{w}_1^{(2)}, \dots, \mathbf{w}_n^{(2)}\}$. To classify an image, we first compute its DCNN output \mathbf{x} . Then for $\mathbf{P}^{(1)T}(f(\mathbf{W}^{(1)}\mathbf{x}) - \frac{1}{n}\sum_i \mathbf{f}_i)$, we compute its k closest columns of $\mathbf{P}^{(2)T}\mathbf{W}^{(2)}$ (seen) and/or $\mathbf{P}^{(2)T}\mathbf{W}^{(3)}$ (unseen). The corresponding classes of these k columns are the top- k predictions. The closeness is measured by cosine similarity. For $\mathbf{W}^{(1)}$, we can use \mathbf{I} (original), \mathbf{U} (whitening) or \mathbf{W} (ICA). For $\mathbf{W}^{(2)}$ and $\mathbf{W}^{(3)}$, we use the feature vectors by running classic Multi-dimensional Scaling (MDS) on a distance matrix of both seen and unseen classes. The distance between two classes is measured by one minus the similarity in Section 4.3. Each column of $\mathbf{W}^{(2)}$ and $\mathbf{W}^{(3)}$ is subtracted by $\frac{1}{n}\sum_i \mathbf{w}_i^{(2)}$. \mathbf{M} is approximated by \mathbf{I} and $f(\cdot)$ is the normalization of a vector or each column of a matrix to unity l_1 norm. We experimented with softmax with different T and normalized logits as the outputs. The best performance (Table 3, 4, 5) was obtained with the softmax ($T = 1$) output for \mathbf{x} but \mathbf{U} and \mathbf{W} were learnt with normalized logits.

Following the zero-shot learning experimental procedures of DeVISE and conSE, we use a DCNN trained on ImageNet ILSVRC2012 (1000 seen classes) described in Section 4.1 as the baseline, and test our method to classify images in ImageNet 2011fall (20842 unseen classes⁴, 21841 both seen and unseen classes). We use top- k accuracy (also called flat hit@ k in [19, 20]) measure, the percentage of test images in which a method’s top- k predictions return the true label. In Table 3, we show the results of three methods on ImageNet 2011fall. Our method outperforms DeVISE and conSE, especially for test set Both (seen and unseen classes). In Table 4, we show the results of the three zero-shot learning methods on the test images selected in [20]. Our method gives correct or reasonable predictions. In Table 5, we show the results of three methods on ImageNet ILSVRC2012 validation set of 1000 seen classes. While the goal here is not to classify images of seen classes, it is desirable to measure how much accuracy a zero-shot learning method would lose compared to the softmax baseline. In Table 3 and 5, we show the dimensionality of image representation for each method in the parenthesis.

With whitening or ICA, our method only loses a small amount of accuracy even with a low dimensional representation (100-dim) of each image, which is useful for situations requiring efficient storage and computation. The results also indicate that, in our zero-shot learning method, whitening could achieve the same performance as ICA, which has much higher computation costs.

As stated in [20], both DeVISE and conSE tend to predict the seen labels more often than the unseen, especially at their first few predictions. Therefore, their performance drops drastically in the Both test set. Our method seems not suffering from the same problem. This might be due to that CCA projects the visual and the semantic representations of object classes into a common space, in where comparisons between visual and semantic data points are more sensible.

Table 3: Top- k accuracy in ImageNet 2011fall zero-shot learning task (%)

Test Set	#Classes	#Images	Method	Top-1	Top-2	Top-5	Top-10	Top-20
Unseen	20842	12.9 million	DeVISE (500-dim)	0.8	1.4	2.5	3.9	6.0
			ConSE (500-dim)	1.4	2.2	3.9	5.8	8.3
			Ours (original, 1000-dim)	1.7	2.8	4.9	6.9	9.2
			Ours (whitening, 999-dim)	1.7	2.8	4.9	6.9	9.3
			Ours (whitening, 500-dim)	1.7	2.8	5.0	7.0	9.4
			Ours (whitening, 100-dim)	1.5	2.5	4.3	6.1	8.2
			Ours (ICA, 999-dim)	1.7	2.8	4.9	6.9	9.3
			Ours (ICA, 500-dim)	1.7	2.8	5.0	7.0	9.4
			Ours (ICA, 100-dim)	1.5	2.5	4.3	6.1	8.2
Both	21841	14.2 million	DeVISE (500-dim)	0.3	0.8	1.9	3.2	5.3
			ConSE (500-dim)	0.2	1.2	3.0	5.0	7.5
			Ours (original, 1000-dim)	6.9	8.7	11.4	13.6	16.1
			Ours (whitening, 999-dim)	6.9	8.7	11.4	13.6	16.1
			Ours (whitening, 500-dim)	6.9	8.6	11.3	13.6	16.2
			Ours (whitening, 100-dim)	6.8	8.2	10.3	12.2	14.5
			Ours (ICA, 999-dim)	6.9	8.7	11.4	13.6	16.1
			Ours (ICA, 500-dim)	6.9	8.6	11.3	13.6	16.2
			Ours (ICA, 100-dim)	6.9	8.2	10.3	12.2	14.5

⁴Class *teddy, teddy bear* (WordNet ID: n04399382) is in ImageNet ILSVRC2012 but not in ImageNet 2011fall. The authors of [19, 20] confirmed us that in their experiments class *teddy, teddy bear* was not included in the two test sets. Thus, the correct number of classes is $21841 - (1000 - 1) = 20842$ rather than 20841.

Table 4: Predictions of test images of unseen classes (correct class labels are in blue)



Test Images	DeViSE [19]	ConSE [20]	Our Method
	water spaniel tea gown bridal gown, wedding gown spaniel tights, leotards	business suit dress, frock hairpiece, false hair, postiche swimsuit, swimwear, bathing suit kit, outfit	periwig, peruke mink, mink coat tights, leotards quack-quack horsehair wig
	heron owl, bird of Minerva, bird of night hawk bird of prey, raptor, raptorial bird finch	ratite, ratite bird, flightless bird peafowl, bird of Juno common spoonbill New World vulture, cathartid Greek partridge, rock partridge	ratite, ratite bird, flightless bird kiwi, apteryx moa elephant bird, aepyornis emu, Dromaius novaehollandiae
	elephant turtle turtleneck, turtle, polo-neck flip-flop, thong handcart, pushcart, cart, go-cart	California sea lion Steller sea lion Australian sea lion South American sea lion eared seal	fur seal ⁵ eared seal fur seal ⁶ guadalupe fur seal Alaska fur seal
	golden hamster, Syrian hamster rhesus, rhesus monkey pipe shaker American mink, Mustela vison	golden hamster, Syrian hamster rodent, gnawer Eurasian hamster rhesus, rhesus monkey rabbit, coney, cony	golden hamster, Syrian hamster Eurasian hamster prairie dog, prairie marmot skink, scincid, scincid lizard mountain skink
	truck, motortruck skidder tank car, tank automatic rifle, machine rifle trailer, house trailer	flatcar, flatbed, flat truck, motortruck tracked vehicle bulldozer, dozer wheeled vehicle	skidder bulldozer, dozer farm machine cultivator, tiller angledozer
	kernel littoral, littoral, littoral zone, sands carillon Cabernet, Cabernet Sauvignon poodle, poodle dog	dog, domestic dog domestic cat, house cat schnauzer Belgian sheepdog domestic llama, Lama peruana	mastiff Seeing Eye dog guide dog alpaca, Lama pacos domestic llama, Lama peruana

Table 5: Top-*k* accuracy in ImageNet ILSVRC2012 validation set (%)

Test Set	#Classes	#Images	Method	Top-1	Top-2	Top-5	Top-10
Seen	1000	50000	Softmax baseline	55.6	67.4	78.5	85.0
			DeViSE (500-dim)	53.2	65.2	76.7	83.3
			ConSE (500-dim)	54.3	61.9	68.0	71.6
			Ours (softmax baseline)	62.7	74.3	84.5	89.6
			Ours (original, 1000-dim)	62.7	74.3	84.5	89.6
			Ours (whitening, 999-dim)	62.7	74.2	84.5	89.5
			Ours (whitening, 500-dim)	62.6	73.8	82.9	87.3
			Ours (whitening, 100-dim)	62.4	72.2	80.8	85.6
			Ours (ICA, 999-dim)	62.7	74.2	84.4	89.5
			Ours (ICA, 500-dim)	62.6	73.8	82.9	87.3
			Ours (ICA, 100-dim)	62.4	72.3	80.8	85.6

6 Conclusion

We showed that the visual features, or label embedding, of object classes can be learned with one-hot class labels and without any human annotated visual attribute label, using both supervised learning (DCNN) and unsupervised learning (PCA/ICA). These visual features were shown to be useful for a new zero-shot learning method proposed in this paper, which outperforms previous state-of-the-art methods.

Acknowledgements

We thank Aapo Hyvarinen and Michael Gutmann for helpful discussions.

⁵WordNet ID: n02077152. There are two classes named *fur seal* with different WordNet IDs.

⁶WordNet ID: n02077658.

Reference

- [1] Yann LeCun, Léon Bottou, Yoshua Bengio, and Patrick Haffner. Gradient-based learning applied to document recognition. *Proceedings of the IEEE*, 1998.
- [2] Dan Ciresan, Ueli Meier, and Jürgen Schmidhuber. Multi-column deep neural networks for image classification. *Computer Vision and Pattern Recognition, IEEE Conference on*, 2012.
- [3] Alex Krizhevsky, Ilya Sutskever, and Geoffrey E Hinton. Imagenet classification with deep convolutional neural networks. *Advances in neural information processing systems*, 2012.
- [4] Charles F Cadieu, Ha Hong, Daniel LK Yamins, Nicolas Pinto, Diego Ardila, Ethan A Solomon, Najib J Majaj, and James J DiCarlo. Deep neural networks rival the representation of primate it cortex for core visual object recognition. *PLoS computational biology*, 2014.
- [5] Geoffrey E Hinton, Oriol Vinyals, and Jeff Dean. Distilling the knowledge in a neural network. *NIPS Deep Learning Workshop*, 2014.
- [6] Aapo Hyvärinen, Juha Karhunen, and Erkki Oja. *Independent component analysis*. John Wiley & Sons, 2004.
- [7] Jia Deng, Wei Dong, Richard Socher, Li-Jia Li, Kai Li, and Li Fei-Fei. Imagenet: A large-scale hierarchical image database. *Computer Vision and Pattern Recognition, IEEE Conference on*, 2009.
- [8] Aapo Hyvarinen. Fast and robust fixed-point algorithms for independent component analysis. *Neural Networks, IEEE Transactions on*, 1999.
- [9] Aapo Hyvarinen. Sparse code shrinkage: Denoising of nongaussian data by maximum likelihood estimation. *Neural computation*, 1999.
- [10] Matthew D Zeiler and Rob Fergus. Visualizing and understanding convolutional networks. *European Conference on Computer Vision*, 2014.
- [11] James Bergstra, Olivier Breuleux, Frédéric Bastien, Pascal Lamblin, Razvan Pascanu, Guillaume Desjardins, Joseph Turian, David Warde-Farley, and Yoshua Bengio. Theano: a CPU and GPU math expression compiler. *Proceedings of the Python for Scientific Computing Conference*, 2010.
- [12] Zeynep Akata, Florent Perronnin, Zaid Harchaoui, and Cordelia Schmid. Label-embedding for attribute-based classification. *Computer Vision and Pattern Recognition, IEEE Conference on*, 2013.
- [13] Thomas Deselaers and Vittorio Ferrari. Visual and semantic similarity in imagenet. *Computer Vision and Pattern Recognition, IEEE Conference on*, 2011.
- [14] Christiane Fellbaum. *WordNet: An Electronic Lexical Database*. Bradford Books, 1998.
- [15] Carlo Baldassi, Alireza Alemi-Neissi, Marino Pagan, James J DiCarlo, Riccardo Zecchina, and Davide Zoccolan. Shape similarity, better than semantic membership, accounts for the structure of visual object representations in a population of monkey inferotemporal neurons. *PLoS computational biology*, 2013.
- [16] Hugo Larochelle, Dumitru Erhan, and Yoshua Bengio. Zero-data learning of new tasks. *AAAI*, 2008.
- [17] Christoph H Lampert, Hannes Nickisch, and Stefan Harmeling. Learning to detect unseen object classes by between-class attribute transfer. *Computer Vision and Pattern Recognition, IEEE Conference on*, 2009.
- [18] Mark Palatucci, Dean Pomerleau, Geoffrey E Hinton, and Tom M Mitchell. Zero-shot learning with semantic output codes. *Advances in neural information processing systems*, 2009.
- [19] Andrea Frome, Greg S Corrado, Jon Shlens, Samy Bengio, Jeff Dean, Tomas Mikolov, et al. Devise: A deep visual-semantic embedding model. *Advances in Neural Information Processing Systems*, 2013.
- [20] Mohammad Norouzi, Tomas Mikolov, Samy Bengio, Yoram Singer, Jonathon Shlens, Andrea Frome, Greg S Corrado, and Jeffrey Dean. Zero-shot learning by convex combination of semantic embeddings. *International Conference on Learning Representation*, 2014.
- [21] Tomas Mikolov, Kai Chen, Greg Corrado, and Jeffrey Dean. Efficient estimation of word representations in vector space. *International Conference on Learning Representation*, 2013.
- [22] David Hardoon, Sandor Szedmak, and John Shawe-Taylor. Canonical correlation analysis: An overview with application to learning methods. *Neural computation*, 2004.